APRIL 2014 VOL 7 NO 4
www.nature.com/naturegeoscience

nature geoscience

ANCIENT OCEAN OXYGEN
Brought to depth by complex life?

INDIAN MONSOON
Desert dust and summer rain

ANDES DEFORMATION
Continental sliver control

Mercury's surface scarred by contraction

nature geoscience

ARTICLES

PUBLISHED ONLINE: 16 MARCH 2014 | DOI: 10.1038/NGEO2097

Mercury's global contraction much greater than earlier estimates

Paul K. Byrne[1,2*†], Christian Klimczak[1], A. M. Celâl Şengör[3], Sean C. Solomon[1,4], Thomas R. Watters[5] and Steven A. Hauck, II[6]

Mercury, a planet with a lithosphere that forms a single tectonic plate, is replete with tectonic structures interpreted to be the result of planetary cooling and contraction. However, the amount of global contraction inferred from spacecraft images has been far lower than that predicted by models of the thermal evolution of the planet's interior. Here we present a synthesis of the global contraction of Mercury from orbital observations acquired by the MESSENGER spacecraft. We show that Mercury's global contraction has been accommodated by a substantially greater number and variety of structures than previously recognized, including long belts of ridges and scarps where the crust has been folded and faulted. The tectonic features on Mercury are consistent with models for large-scale deformation proposed for a globally contracting Earth—now obsolete—that pre-date plate tectonics theory. We find that Mercury has contracted radially by as much as 7 km, well in excess of the 0.8–3 km previously reported from photogeology and resolving the discrepancy with thermal models. Our findings provide a key constraint for studies of Mercury's thermal history, bulk silicate abundances of heat-producing elements, mantle convection and the structure of its large metallic core.

Global contraction as a result of interior cooling was invoked as an explanation for mountain building and tectonic deformation on Earth in the nineteenth century[1,2], but the idea was abandoned even before the recognition of the horizontal mobility of tectonic plates[3], with the realization that contraction cannot account for the amount, style and distribution of deformation on the Earth's surface[4]. Large-scale deformational systems on Earth are localized along plate margins, unlike the quasi-homogenous distribution of shortening structures predicted for a contracting planet[3].

However, other worlds in the Solar System do not exhibit plate tectonics today, so the intriguing possibility exists that some of the old concepts of contraction theory for global tectonics, long obsolete for Earth, may be valid for one-plate planets. Mercury, in particular, displays no evidence of plate boundaries that segment its globally continuous lithosphere. Yet observations made by the Mariner 10 and MErcury Surface, Space ENvironment, GEochemistry, and Ranging (MESSENGER) spacecraft have shown that the innermost planet displays myriad landforms—lobate scarps, wrinkle ridges and high-relief ridges—that have been interpreted as the tectonic result of horizontal shortening of the lithosphere as Mercury contracted in response to secular cooling of its interior[5–9].

Still, important details of Mercury's contraction, such as the timing, duration and spatial concentration of surface deformation, have remained elusive. Until the MESSENGER flybys of Mercury in 2008–2009, an entire hemisphere of Mercury had yet to be imaged, so inferences made on the basis of Mariner 10 data could not reliably be generalized globally. Furthermore, widespread topographic data for the planet were not available until MESSENGER began orbital operations at Mercury in 2011, thus limiting the accuracy of earlier estimates of the amount of planetary contraction accommodated by surface structures. Determining the extent to which Mercury contracted is key to understanding the planet's thermal, tectonic and volcanic history. Earlier estimates of Mercury's radial contraction since the last major episode of global resurfacing (by impact cratering and/or widespread volcanism[10]) obtained from photogeological studies of tectonic landforms[5,8,9,11,12] were in the range 0.8–3 km, substantially less than the ∼5–10 km predicted by interior thermal history models[13–15].

The key to addressing these outstanding problems is to characterize how contraction is manifest on Mercury through photogeological mapping of the entire planet, in as detailed a manner as current MESSENGER data allow. Here, we present the results of the most comprehensive survey yet of Mercury's global contraction-induced tectonic features formed since the end of the late heavy bombardment (LHB) of the inner Solar System. We report the distribution, morphology and likely kinematic development of four classes of shortening structure on the planet. In quantifying the surface expression of global contraction on Mercury, we note conceptual similarities between our observations of large-scale crustal deformation on Mercury and explanations offered for a globally contracting Earth before the ascendance of plate tectonics theory. From two complementary methods, we show that the planet experienced much greater contraction than has heretofore been recognized. Our results resolve a decades-old paradox in our understanding of Mercury's geological history and provide the basis for a general framework for investigating global tectonics on other one-plate planets.

[1]Department of Terrestrial Magnetism, Carnegie Institution of Washington, Washington, DC 20015, USA, [2]Lunar and Planetary Institute, Universities Space Research Association, Houston, Texas 77058, USA, [3]Department of Geology, Faculty of Mines and the Eurasia Institute of Earth Sciences, Istanbul Technical University, 34469 Maslak, Istanbul, Turkey, [4]Lamont-Doherty Earth Observatory, Columbia University, Palisades, New York 10964, USA, [5]Center for Earth and Planetary Studies, National Air and Space Museum, Smithsonian Institution, Washington, DC 20560, USA, [6]Department of Earth, Environmental, and Planetary Sciences, Case Western Reserve University, Cleveland, Ohio 44106, USA. †Present address: Lunar and Planetary Institute, Universities Space Research Association, Houston, Texas 77058, USA. *e-mail: pbyrne@carnegiescience.edu

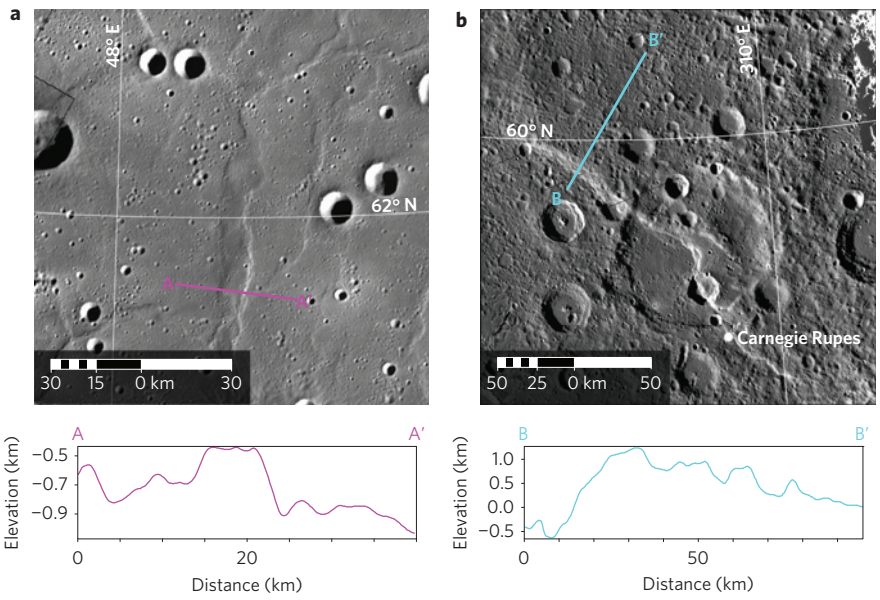

Figure 1 | Primary styles of thrust faulting on Mercury. **a**, A typical wrinkle ridge in the northern volcanic plains[20]; a topographic profile (along the line A–A′ shown in the top panel) shows its characteristic ridge-like morphology. **b**, Carnegie Rupes, a lobate scarp in Mercury's northern hemisphere; in cross-section the structure is a steep, convex escarpment. Note the difference in vertical relief across the two structures. Profiles are from MDIS stereo digital terrain models[49]; elevation values here and in subsequent figures are relative to a sphere of 2,440 km radius[32]. Azimuthal equidistant projections centred at 61.4° N, 49.9° E (**a**) and 59.1° N, 304.5° E (**b**).

Classes of shortening structures

Early descriptions of contractional deformation on Earth included two dominant styles of deformation. Large, stable regions (cratons), outlined by mobile belts, are subject to shortening by means of deeply rooted thrust faults (termed germanotype faults[16]) that extend far into their interior. In contrast, the belts themselves are composed of smaller, more densely grouped alpinotype faults[16], some of which may root into the deeper structures. A third, now conceptually abandoned, type of shortening structure on Earth consisted of geosynclines and geanticlines, complementary long-wavelength fold structures that were hypothesized to deform the entire lithosphere and were invoked to account for the immense thicknesses of shallow-water sedimentary rocks observed in mountain belts[1,2].

In 1974–1975, Mariner 10 data revealed two primary tectonic expressions of horizontal shortening on Mercury[5]. Wrinkle ridges are typically broad, low-relief arches—essentially an anticlinal fold above a blind thrust fault—often superposed by a narrow ridge (Fig. 1a). Lobate scarps are characterized by a steeply sloping scarp face and a gently sloping back limb, probably represent a monocline or asymmetric hanging-wall anticline atop a blind or surface-breaking thrust fault and are generally larger and presumably accommodated more shortening than wrinkle ridges (Fig. 1b). (A less common form of scarp is known as a high-relief ridge.) Intriguingly, long-wavelength undulations of Mercury's topography have been identified in data returned by MESSENGER[17]—and so it may be that Mercury's wrinkle ridges correspond to the alpinotype faults described on Earth, its larger lobate scarps are their germanotype counterparts and the long-wavelength topographic undulations on Mercury may possibly be analogues to the long-discarded geosyncline and geanticline paradigm for Earth[1,2].

To fully document the global contraction of Mercury and so test these inferences, we identified 5,934 ridges and scarps that we attribute to global contraction, together with a number of long-wavelength topographic undulations (Fig. 2). Individual fault-related features range from ~9 to 900 km in length and their cumulative length is 4.16×10^8 m (Supplementary Table 1). In contrast to previous mapping studies that separated wrinkle ridges, lobate scarps and high-relief ridges (for example, ref. 9), here most mapped shortening structures are classified by the primary terrain type—smooth plains[18] or cratered plains (a term we use to refer to both the intercrater plains and heavily cratered terrain units described from Mariner 10 images[19])—in which they occur. Under this approach, most mapped landforms are classified as smooth plains structures or cratered plains structures (Supplementary Fig. 1). The remaining structures are either spatially associated with impact craters and so are termed crater-related or border areas of high-standing terrain and are catalogued as high-terrain bounding. Long-wavelength undulations are mapped as either troughs or crests on the basis of their elevation relative to surrounding terrain and the directions of tilt of crater floors on their flanks (Fig. 2). These structure classes are described in greater detail in the accompanying Supplementary Discussion.

Regional-scale crustal deformation

Shortening-related faulting is not uniformly distributed on Mercury. The northern volcanic plains, representing just ~6% of the planet's surface[20], host a disproportionately large number of contractional landforms (1,668, or 28% of the mapped total and 19% of the cumulative length). The relative youth of these plains[20] may aid in the recognition of superposed tectonic structures, however, compared with those located in cratered terrain. The remaining structures show no clear evidence of a globally coherent lithospheric fracture pattern that survived the LHB (ref. 10), such as that predicted to have been influenced by tidal despinning[6,21]. We do note, however, that our structural survey is likely to have been influenced at least in part by lighting geometry (Supplementary Discussion and Supplementary Fig. 2).

Nonetheless, there is evidence of systematic regional-scale deformation on Mercury. In places, groups of ridges and scarps form laterally contiguous, narrow bands of considerable length. One such system, shown in Fig. 3, extends for some 1,700 km (over 40° of arc) across Mercury's northern hemisphere and includes Victoria and Endeavour Rupēs and Antoniadi Dorsum. Many of its constituent

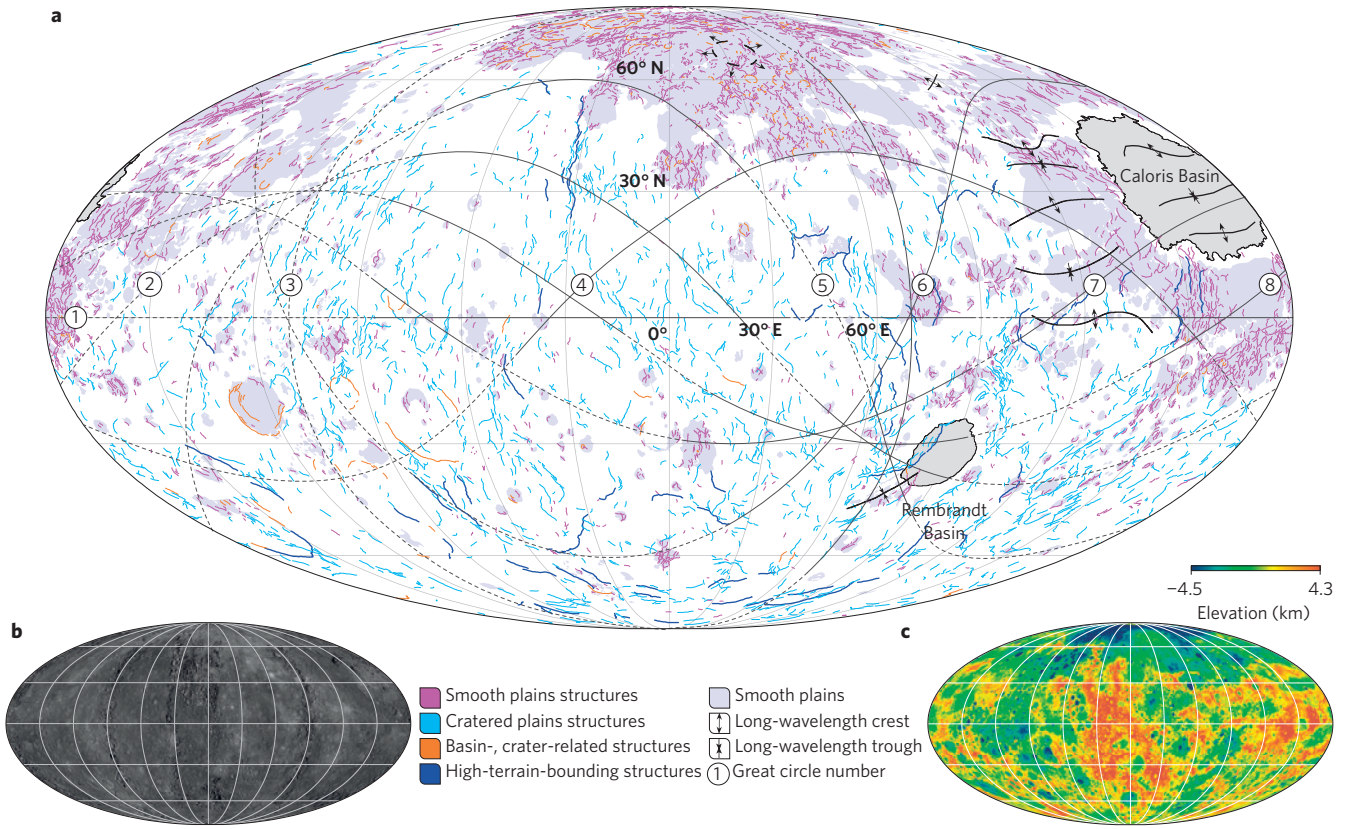

Figure 2 | Shortening structures on Mercury. **a**, The 5,934 classified thrust-fault-related landforms of this study; mapped smooth plains[29] are shown, as are the Caloris and Rembrandt basins. Black lines mark the crests (opposing arrows) and troughs (facing arrows) of mapped long-wavelength topographic undulations. Measurements were taken along the unbroken portions of great circles 1–8. **b**,**c**, The global MDIS combined high-incidence-angle and monochrome base map (**b**) and topography derived from the controlled MDIS wide-angle camera base map[49] (**c**) used here. Each map is in a Mollweide projection centred at 0°; graticule shown in 30° increments.

landforms are cratered plains structures, but those that comprise its northern portion border an area of high-standing terrain to the west and show evidence of displacement (that is, vergence) eastwards onto the adjacent smooth plains. This sense of vergence is echoed by the other high-terrain-bounding structures along its length. An even longer system, 1,800 km long, extends from 19° N, 55° E to 23° S, 61° E and also has a dominant (westwards) vergence.

We therefore regard these systems as Mercury's equivalent of fold-and-thrust belts (FTBs) on Earth[22] and Venus[23], which in their simplest terms are linear, regionally contiguous sets of thrust faults with associated hanging-wall anticlines that have a single predominant sense of vergence. Many FTBs on Earth feature an extensive décollement at depth[24,25]; whether this structural arrangement exists for Mercury's FTBs remains to be tested, but detachments have been proposed to underlie individual, highly arcuate large lobate scarps on the planet[26].

Kinematics of shortening-related deformation

The contrast in morphology and density of tectonic structures hosted by the younger smooth plains and the older cratered plains (Figs 1 and 2) could reflect differences in rheological and structural fabric characteristics between the two terrain types[8,27]. Analyses of MESSENGER X-Ray Spectrometer and Gamma-Ray Spectrometer data indicate that the surface composition of at least some heavily cratered terrain is more magnesian but less feldspathic than the low-iron basalt-like northern volcanic plains[28]. With their internal structure rendered more complex by sustained impacts and volcanic resurfacing[29], the cratered plains material may thus have massive textures that facilitated the development of thick-skinned, large-scale fault systems that root to depths of tens of kilometres (and possibly to deep basal décollements), consistent with the results of forward modelling studies of topographic profiles across several lobate scarps[8].

In contrast, the smooth plains probably feature strong vertical variation in mechanical properties inherent to layered volcanic strata that promote detachments and thin-skinned tectonic deformation. Wrinkle ridges occur consistently within stratified units on Mars and, although there is debate as to whether those structures are thick- or thin-skinned in nature[30] and what subsurface structural architecture governs their complex surface morphologies[31], fits of elastic dislocation models to topographic profiles indicate that their thrust faults root to shallow crustal levels[27]. Given the similarity in setting and morphology between wrinkle ridges on Mars and Mercury, smooth plains landforms on the latter body are probably thin-skinned structures that root to décollements (some combination of the interface between the smooth plains and the underlying megaregolith basement and interbeds within the plains deposits themselves[27]).

Where ridges and scarps demarcate buried impact craters in smooth plains (Supplementary Fig. 1), such features probably formed by the localization of compressive stresses above crater rims[9]. In contrast, outward-verging lobate scarps within impact basin rims may represent partitioning of shortening strain between the basin and its interior smooth fill, either as a result of a difference in elastic moduli (or yield strength) between the fill and basin floor material or, as for the smooth plains structures, by the rooting of scarp faults into a décollement between the two deposits.

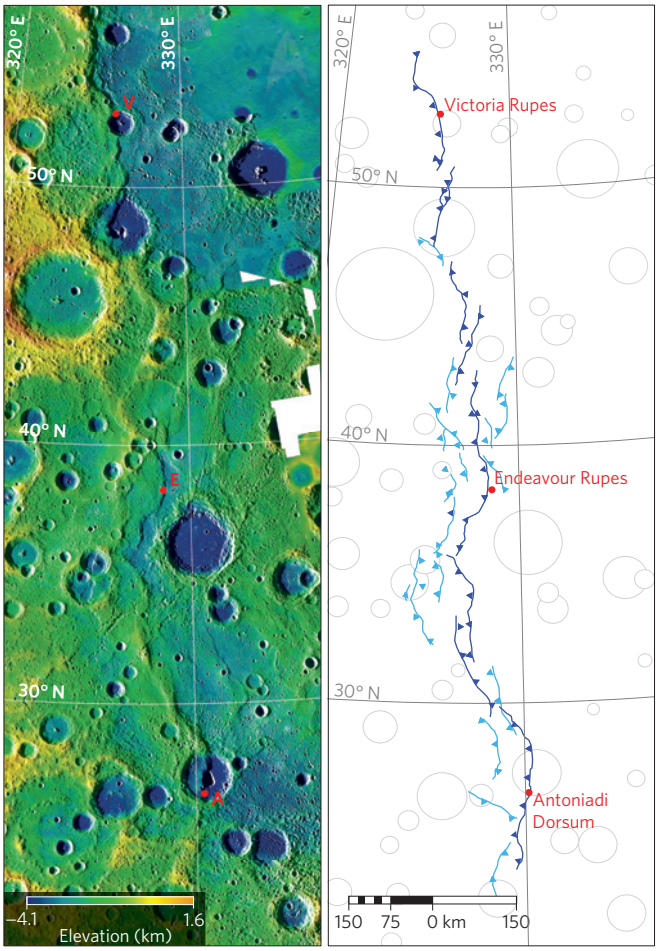

Figure 3 | A Mercury fold-and-thrust belt (FTB). One of the most prominent FTBs documented on Mercury, this system is ~1,700 km long and consists of an assemblage of lobate scarps and high-relief ridges. Named parts of this system include Victoria (V) and Endeavour (E) Rupes and Antoniadi Dorsum (A). Left panel: MDIS stereo digital terrain model[49] overlaid on the MDIS global basemap. Right panel: surface traces of structures (arrows indicate down-dip direction), colour-coded as in Fig. 2 and with pronounced craters outlined in grey. Azimuthal equidistant projection centred at 40° N, 328° E.

Regions of high- and low-standing terrain on Mercury do not seem to correlate spatially with free-air gravity anomalies over the planet's northern hemisphere, a result indicating that topography is largely isostatically compensated, presumably by variations in crustal thickness[32]. Those tectonic structures that border high-standing terrain may therefore have isolated thicker crustal blocks from neighbouring, thinner portions of the crust, localizing substantial lithospheric shortening along their length, penetrating far into the crust and accumulating considerable strain (resulting in relief of up to several kilometres, such as that for Enterprise Rupes, shown in Supplementary Fig. 1). With continued shortening, thicker crustal blocks overthrust adjacent low-lying terrain as on Earth[33,34]. Moreover, where smooth plains structures are located adjacent to and share a dominant direction of displacement with highland-bounding and cratered plains structures, the smaller alpinotype-like landforms may root into the germanotype-like faults—a structural arrangement seen in the Alps[35], the European Hercynides[36], the Appalachian–Ouachita orogen[37], the Himalaya[38], the US Rockies[39] and the Andes[40].

If characteristics of long-wavelength undulations across the planet resemble those of the abandoned geosyncline and geanticline hypothesis for Earth[2], this warping may reflect lithospheric buckling or folding[7,15] in response to the global contraction that accompanied interior cooling. However, the horizontal strains accommodated by folds of such observed wavelengths and amplitudes may be of the order of 10^{-5} (ref. 41), so their contribution to planetary radius change would be minor compared with that of the fault-related structures. Such buckling on Earth and presumably Mercury requires compressional stresses that substantially exceed the elastic strength of the lithosphere. Models of an elastic–plastic lithosphere, however, allow for folding far below the threshold of elastic buckling stresses[42].

It is possible that these undulations are the result of mantle dynamic processes[43], consistent with convective thermal models of Mercury's interior (including those in which mantle convection continues to the present[44]). Three-dimensional models of convection within Mercury's thin mantle predict convection patterns characterized by long, sheet-like shapes and a polygonal pattern near the intersection of the sheet structures[43]; to first-order, the linear undulations shown in Fig. 2 are consistent with this pattern. However, the amplitude of dynamic topography predicted by models with these patterns is one to two orders of magnitude[43] below that of observed undulations[41].

The origin of Mercury's long-wavelength warping thus remains unclear. Whatever the provenance of these undulations, an important additional observation is that in several instances the warping seems to postdate the emplacement of the youngest expanses of smooth plains on Mercury[41] (that is, the northern and Caloris interior plains). This relation indicates that long-wavelength modification of the planet's topography occurred more recently than 3.8 Gyr ago[41]—placing an important temporal constraint on the causal mechanism(s) responsible.

Planetary radius change

From our global survey of mapped structures, we estimated the accumulated decrease in Mercury's radius accommodated by mapped structures with two complementary techniques (Methods). With the first approach, we summed the individual estimates of horizontal shortening across 216 structures intersected by eight great circles. For an assumed dip angle (θ) of 25°, 30° and 35° for the thrust faults underlying each contractional landform, this method gives a mean change in planetary radius of 5.5 km, 4.4 km and 3.7 km, respectively (Table 1).

To enable a direct comparison between this work and preceding studies of Mercury's global contraction[8,11,12], we also used those same 216 structures to define a scaling factor (γ) between maximum fault displacement (D_{max}) and fault length (L) for extrapolation to all mapped landforms (following the methodology of ref. 11). The D_{max}–L method has the benefit of considering all of the structures in Fig. 2 and so we consider it more representative of the record of radial shortening preserved on Mercury. After subtracting the surface areas of Caloris and Rembrandt basins, for which interior structures were not included in the analysis, we calculated radius change values of 7.1 km, 5.7 km and 4.7 km for the same three values of θ as those adopted for the first method (Table 1). Although smooth plains structures have been attributed to global contraction in some studies, they have also been at least partially ascribed to load-induced flexure and subsidence and have been excluded from estimates of global contraction in other investigations. We therefore also estimated values of radial contraction with no smooth plains structures included. When the surface area of smooth plains (~27% of the total planetary surface) is excluded, together with that of the Caloris and Rembrandt interiors, the change in planetary radius for $\theta = 25°$, 30° and 35° is 6.3 km, 5.1 km and 4.2 km, respectively (Table 1).

Although these estimates of radius change differ by 1–1.6 km, values obtained by both methods are substantially greater than

Table 1 | Planetary radius change from the great circle and displacement–length scaling methods.

Great circle method								
Great circle number	Number of structures	Normal no. 1		Normal no. 2		Radius change (km) for given dip angle		
		Lat (°)	Lon (°)	Lat (°)	Lon (°)	25°	30°	35°
1	42	90 N	0 E	90 S	180 E	6.7	5.4	4.5
2	28	50 N	110 E	50 S	290 E	5.2	4.2	3.5
3	21	0 N	160 E	0 N	340 E	4.9	4.0	3.3
4	24	50 S	60 E	50 N	240 E	5.7	4.6	3.8
5	18	30 N	140 E	30 S	320 E	5.7	4.6	3.8
6	25	30 S	160 E	30 N	340 E	4.3	3.5	2.9
7	33	60 N	20 E	60 S	200 E	6.6	5.3	4.4
8	25	60 N	70 E	60 S	250 E	4.6	3.7	3.1
Mean	27					5.5	4.4	3.7
Displacement–length scaling method								
Fault plane dip angle						25°	30°	35°
Derived value of γ						9.6×10^{-3}	8.1×10^{-3}	7.1×10^{-3}
Radius change from all structures (5,934) (km)								
Surface area of Mercury (7.48×10^{13} m^2)						6.9	5.6	4.6
Surface area excluding the Caloris and Rembrandt basin interiors (7.27×10^{13} m^2)						7.1	5.7	4.7
Radius change excluding smooth plains structures (2,183) (km)								
Surface area of Mercury (7.48×10^{13} m^2)						4.6	3.7	3.1
Surface area excluding smooth plains and the Caloris and Rembrandt basin interiors (5.46×10^{13} m^2)						6.3	5.1	4.2

those from earlier photogeological studies[5,8,11,12]. Previous reports of 0.8–2 km of radial shortening[5,8,11] were derived from analyses of the 45% of Mercury's surface imaged by Mariner 10. A recent D_{max}–L study[44] using MESSENGER data considered only the most prominent lobate scarps and high-relief ridges on Mercury and returned a value of ~1.2 km for $\theta = 30°$. Even the highest previously reported value for radius change[12] (3 km for $\theta = 30°$) was based on an analysis of only 21% of Mercury's surface that was then extrapolated to the entire planet, and that study adopted a D_{max}/L ratio derived from only eight lobate scarps imaged by Mariner 10 (ref. 11). In comparison, our D_{max}–L analysis, obtained with a scaling relation derived from 27 times as many structures and applied to the entire population of shortening structures on Mercury, gives a value for radial contraction of 5.7 km (5.1 km if smooth plains structures are excluded) for $\theta = 30°$. Even these estimates of radius change accommodated by contractional landforms are likely to underestimate the actual extent of Mercury's global contraction since the LHB, because of limitations on illumination geometry in many areas of the base map used in this study (Supplementary Discussion).

Our results provide an important new constraint for understanding the thermal history of Mercury's interior. MESSENGER orbital measurements of the relative surface abundances of K/Th and Th/U (the main heat-producing elements in planetary interiors) indicate larger fractions of K and U and their comparatively shorter-lived isotopes than have been used so far in thermal evolution studies[45]. It is therefore likely that Mercury experienced a greater change in heat production since the LHB (and so has cooled more) than previous models suggest, further exacerbating the discrepancy between theoretical findings and previous photogeological observations. That we have documented changes in Mercury's radius of up to a factor of seven larger than previous results resolves a nearly four-decades-old paradox: the history of heat production and loss and the accumulated global contraction are now consistent[13–15]. Going forward, our findings are crucial to thermal history models that will address the bulk silicate abundances of heat-producing elements, the question of whether the mantle is convecting[44] at present and the history of cooling and present-day structure of the large metallic core, the source of Mercury's internal magnetic field[7,46].

Moreover, our synthesis of the surface manifestation of global contraction on Mercury provides fresh insight for spatial and temporal studies of volcanism and tectonics on the innermost planet. And with the increasing number of terrestrial planets identified in extrasolar planetary systems[47], Mercury may come to serve as a case study with which to understand the global cooling and contractional histories of rocky, one-plate planets in general.

Methods

Data. We produced the global thrust fault map in Fig. 2 from a combination of Mercury Dual Imaging System (MDIS; ref. 48) monochrome and high-incidence-angle global mosaics, obtained during the first and third solar days of MESSENGER's orbital mission, respectively. The mosaics, with a mean resolution of 250 m px^{-1}, were placed within a geographical information system (GIS). Elevation values were taken from laser altimeter[17] and stereophotogrammetric (for example, ref. 49) topographic data sets that were added to the GIS.

Mapping approach. Thrust-fault-related structures were identified and interpreted as such on the basis of their convex-upward morphology, linear-to-arcuate planform and classic thrust-fault-related map patterns (for example, en echelon stepover regions between structures). Surface traces were drawn along sharp breaks in slope at the leading edges of landforms determined to be shortening structures, at a constant view scale of 1:2,000,000 and in such a manner so as to record the vergence of—the direction of displacement along—the inferred underlying thrust fault. This property was determined under the assumption that the leading edge of a tectonic landform is the steeper flank of a thrust-fault-related fold, with the tilt of the axial plane of that fold indicative of the direction of slip along the underlying fault. (We note, however, that

uncertainty exists in at least some cases when inferring fault dip direction from the surface asymmetry of a thrust-fault-related landform[30,31].) Care was taken to exclude non-tectonic lineations such as impact-sculpted terrain, eroded crater rims or lava flow fronts. Where the nature of a given landform was ambiguous, the feature was not included. We did not investigate contractional tectonics within the volcanic interior plains of Caloris or Rembrandt basins; although these basins host substantial structural complexity, the extent to which those structures are the result of global contraction rather than basin-related processes is not known.

Planetary radius change estimates. We calculated estimates of planetary radial shortening with two complementary methods: first, great circles; and second, displacement–length scaling. Under the first method, eight great circles were positioned at a range of sites on Mercury's surface so as to cross as many tectonic structures on the planet as possible. In the absence of subaerial erosion and under the assumption that the relief of a given landform corresponds to the vertical component (throw, t) of an underlying fault with a planar geometry, the horizontal component (heave, h) of the structure along the great circle was calculated from the relation $h = t\tan^{-1}(\theta)$, where θ is true fault dip angle (Supplementary Fig. 3). (For structures for which the strike direction was not orthogonal to a great circle we determined apparent dip, θ_a, from θ from the relation $\theta_a = \tan^{-1}(\tan(\theta)\sin(\psi))$, where ψ is the angle between the structure's strike direction and the great circle.) Values of $\theta = 25°$, 30° and 35° were adopted when calculating h for the 216 structures crossed by the eight great circles shown in Fig. 2, because these fault dip angles have been used in previous radius-change studies (for example, ref. 12). We measured only those structures along portions of the great circles for which we had topographic data of sufficient resolution (which we regarded as $<1{,}000$ m px^{-1}, shown by the unbroken grey lines in Fig. 2) and we extrapolated the cumulative h values for those portions of the circles to the planetary circumference. The change in planetary radius, ΔR, accommodated along each great circle is then given by $\Delta R = h_{\mathrm{CUMULATIVE}}(2\pi)^{-1}$. These values, together with the positions of the normals to each great circle, are given in Table 1.

Under the second method, we followed the approach described in ref. 11 to estimate planetary radius change using a scaling relation between maximum fault displacement (D_{max}) and fault length (L). We measured the length of, and maximum vertical displacement along, the same 216 structures crossed by the great circles of the first method and, by determining the best-fit linear regression D_{max}–L scaling statistic[50] for these 216 faults, we calculated D_{max}–L ratios (γ), again for $\theta = 25°$, 30° and 35°. We then computed the spherical lengths of all mapped fault traces and found their representative displacements with the scaling relation for the assumed fault dip angles and the respective γ values. Finally, shortening strains and corresponding radius change values were calculated for the entire surface area of Mercury, for that portion of the planet that excludes the Caloris and Rembrandt basins and for the portion that excludes both those basins and the smooth plains[18] (Table 1).

Received 20 July 2013; accepted 23 January 2014; published online 16 March 2014

References

1. De Beaumont, E. L. Faits pour servir a l'histoire des montagnes de l'Oisans. *Mém. Soc. d'Hist. Natur. Paris* **5,** 1–32 (1829).
2. Dana, J. D. On some results of the Earth's contraction from cooling, including a discussion of the origin of mountains and the nature of the Earth's interior. *Am. J. Sci.* **5,** 423–443 (1873).
3. Wilson, J. T. Hypothesis of Earth's behaviour. *Nature* **198,** 925–929 (1963).
4. Dutton, C. E. A criticism of the contractional hypothesis. *Am. J. Sci.* **8,** 113–123 (1874).
5. Strom, R. G., Trask, J. J. & Guest, J. E. Tectonism and volcanism on Mercury. *J. Geophys. Res.* **80,** 2478–2507 (1975).
6. Melosh, H. J. & McKinnon, W. B. in *Mercury* (eds Vilas, F., Chapman, C. R. & Matthews, M. S.) 374–400 (Univ. Arizona Press, 1988).
7. Hauck, S. A. II, Dombard, A. J., Phillips, R. J. & Solomon, S. C. Internal and tectonic evolution of Mercury. *Earth Planet. Sci. Lett.* **222,** 713–728 (2004).
8. Watters, T. R., Robinson, M. S. & Cook, A. C. Topography of lobate scarps on Mercury: New constraints on the planet's contraction. *Geology* **26,** 991–994 (1998).
9. Watters, T. R. *et al.* The tectonics of Mercury: The view after MESSENGER's first flyby. *Earth Planet. Sci. Lett.* **285,** 283–296 (2009).
10. Marchi, S. *et al.* Global resurfacing of Mercury 4.0–4.1 billion years ago by heavy bombardment and volcanism. *Nature* **499,** 59–61 (2013).
11. Watters, T. R. & Nimmo, F. in *Planetary Tectonics* (eds Watters, T. R. & Schultz, R. A.) 15–80 (Cambridge Univ. Press, 2010).
12. Di Achille, G. *et al.* Mercury's radius change estimates revisited using MESSENGER data. *Icarus* **221,** 456–460 (2012).
13. Solomon, S. C. The relationship between crustal tectonics and internal evolution in the Moon and Mercury. *Phys. Earth. Plan. Inter.* **15,** 135–145 (1977).
14. Schubert, G., Ross, M. N., Stevenson, D. J. & Spohn, T. in *Mercury* (eds Vilas, F., Chapman, C. R. & Matthews, M. S.) 429–460 (Univ. Arizona Press, 1988).
15. Dombard, A. J. & Hauck II, S. A Despinning plus global contraction and the orientation of lobate scarps on Mercury: Predictions for MESSENGER. *Icarus* **198,** 274–276 (2008).
16. Stille, H. Über Alter und Art der Phasen variszischer Gebirgsbildung. *Nachr. k. Ges. Will. Göttingen, Math.-Phys. Kl., Jg.* 218–224 (1920).
17. Zuber, M. T. *et al.* Topography of the northern hemisphere of Mercury from MESSENGER laser altimetry. *Science* **336,** 217–220 (2012).
18. Denevi, B. W. *et al.* The distribution and origin of smooth plains on Mercury. *J. Geophys. Res. Planets* **118,** 891–907 (2013).
19. Trask, N. J. & Guest, J. E. Preliminary geologic terrain map of Mercury. *J. Geophys. Res.* **80,** 2461–2477 (1975).
20. Head, J. W. *et al.* Flood volcanism in the northern high latitudes of Mercury revealed by MESSENGER. *Science* **333,** 1853–1856 (2011).
21. Melosh, H. J. & Dzurisin, D. Mercurian global tectonics: A consequence of tidal despinning? *Icarus* **35,** 227–236 (1978).
22. Poblet, J. & Lisle, R. J. Kinematic evolution and styles of fold-and-thrust belts. *Geol. Soc. Lond. Spec. Pub.* **349,** 1–24 (2011).
23. Burke, K. C., Şengör, A. M. C. & Francis, P. W. Maxwell Montes in Ishtar—A collisional plateau on Venus? *Lunar Planet. Sci.* **15,** 104–105 (1984).
24. McClay, K. R. (ed.) *Thrust Tectonics* (Chapman & Hall, 1992).
25. Roeder, D. *American and Tethyan Fold-Thrust Belts* (Gebrüder Borntraeger, 2009).
26. Rothery, D. A. & Massironi, M. Beagle Rupes—Evidence for a basal decollement of regional extent in Mercury's lithosphere. *Icarus* **209,** 256–261 (2010).
27. Watters, T. R. Elastic dislocation modeling of wrinkle ridges on Mars. *Icarus* **171,** 284–294 (2004).
28. Weider, S. Z. *et al.* Chemical heterogeneity on Mercury's surface revealed by the MESSENGER X-Ray Spectrometer. *J. Geophys. Res.* **117,** E00L05 (2012).
29. Denevi, B. W. *et al.* The evolution of Mercury's crust: A global perspective from MESSENGER. *Science* **324,** 613–618 (2009).
30. Mueller, K. & Golombek, M. Compressional structures on Mars. *Annu. Rev. Earth Planet. Sci.* **32,** 435–464 (2004).
31. Schultz, R. A. Localization of bedding plane slip and backthrust faults above blind thrust faults: Keys to wrinkle ridge structure. *J. Geophys. Res.* **105,** 12035–12052 (2000).
32. Smith, D. E. *et al.* Gravity field and internal structure of Mercury from MESSENGER. *Science* **336,** 214–217 (2012).
33. Suess, E. *Das Antlitz der Erde,* Vol. III.2 (Tempsky, Prag & Freytag, 1909).
34. Şengör, A. M. C., Natal'in, B. A. & Burtman, V. S. Evolution of the Altaid tectonic collage and Palaeozoic crustal growth in Eurasia. *Nature* **364,** 299–307 (1993).
35. Trümpy, R. *Geology of Switzerland, A Guide-book. A: An Outline of the Geology of Switzerland* (Schweizerische Geologische Kommission, 1980).
36. Bois, C. *et al.* in *Reflection Seismology: A Global Perspective* (eds Barazangi, M. & Brown, L.) 21–29 (Am. Geophys. Un., 1986).
37. Hatcher, R. D. Jr in *The Appalachian-Ouachita Orogen in the United States, The Geology of North America* (eds Hatcher, R. D. Jr, Thomas, W. A. & Viele, G. W.) 511–535 (Geol. Soc. Am., 1989).
38. McDougall, J. W., Hussain, A. & Yeats, R. S. in *Himalayan Tectonics* (eds Treolar, P. J. & Searle, M. P.) 581–588 (Geol. Soc. Lond. Spec. Pub. 74, 1993).
39. Stille, H. *Einführung in den Bau Amerikas* (Gebrüder Borntraeger, 1940).
40. Roeder, D. Andean-age structure of Eastern Cordillera (Province of La Paz, Bolivia). *Tectonics* **7,** 23–39 (1988).
41. Klimczak, C. *et al.* Insights into the subsurface structure of the Caloris Basin, Mercury, from assessments of mechanical layering and changes in long-wavelength topography. *J. Geophys. Res. Planets* **118,** 2030–2044 (2013).
42. McAdoo, D. C. & Sandwell, D. T. Folding of oceanic lithosphere. *J. Geophys. Res.* **90,** 8563–8569.
43. King, S. D. Pattern of lobate scarps on Mercury's surface reproduced by a model of mantle convection. *Nature Geosci.* **1,** 229–232 (2008).
44. Michel, N. C. *et al.* Thermal evolution of Mercury as constrained by MESSENGER observations. *J. Geophys. Res. Planets* **117,** 1033–1044 (2013).
45. Peplowski, P. N. *et al.* Radioactive elements on Mercury's surface from MESSENGER: Implications for the planet's formation and evolution. *Science* **333,** 1850–1852 (2011).
46. Grott, M., Breuer, D. & Laneuville, M. Thermo-chemical evolution and global contraction of Mercury. *Earth. Planet. Sci. Lett.* **307,** 135–146 (2011).
47. Barclay, T. *et al.* A sub-Mercury-sized exoplanet. *Nature* **494,** 452–454 (2013).
48. Hawkins, S. E. III *et al.* The Mercury Dual Imaging System on the MESSENGER spacecraft. *Space Sci. Rev.* **131,** 247–338 (2007).

49. Becker, K. J. *et al.* Global controlled mosaic of Mercury from MESSENGER orbital images. *Lunar Planet. Sci.* **43,** abstr. 2654 (2012).
50. Clark, R. M. & Cox, S. J. D. A modern regression approach to determining fault displacement-length scaling relationships. *J. Struct. Geol.* **18,** 147–152 (2010).

Acknowledgements

We thank C. M. Ernst and N. L. Chabot (The Johns Hopkins University Applied Physics Laboratory, JHU/APL) for the incidence angle maps shown in Supplementary Fig. 2b,c and H. J. Melosh (Purdue University) for his constructive advice during the preparation of this paper. We also thank W. B. McKinnon for comments that substantially improved this manuscript. The MESSENGER project is supported by the NASA Discovery Program under contracts NASW-00002 to the Carnegie Institution of Washington and NAS5–97271 to JHU/APL. This research has made use of NASA's Astrophysics Data System and Planetary Data System.

Author contributions

P.K.B. and C.K. led the study, carried out data analyses and documented the findings; P.K.B., C.K., A.M.C.S. and S.A.H. wrote the manuscript and P.K.B. prepared the figures. A.M.C.S. led the historical review of the description and interpretation of contractional landforms on Earth. S.C.S. and T.R.W. participated in scientific discussions. All authors contributed to the interpretation of results and to the finalization of the submitted manuscript.

Additional information

Supplementary information is available in the online version of the paper. Reprints and permissions information is available online at www.nature.com/reprints. Correspondence and requests for materials should be addressed to P.K.B.

Competing financial interests

The authors declare no competing financial interests.